^{13}C pNMR of "Crumple Zone" Cu(II) Isophthalate Metal-Organic Frameworks

Daniel M. Dawson[1]*, Charlotte E. F. Sansome[1], Lauren N. McHugh[1], Matthew J. McPherson[1,2], Laura J. McCormick McPherson,[1] Russell E. Morris[1] and Sharon E. Ashbrook[1]*

1. School of Chemistry, EaStCHEM and Centre of Magnetic Resonance, University of St Andrews, St Andrews KY16 9ST, United Kingdom

2. Current address: Energy Safety Research Institute, Swansea University, Fabian Way, Swansea, SA1 8EN

*Authors to whom correspondence should be addressed.

Email: *dmd7@st-andrews.ac.uk*

sema@st-andrews.ac.uk

Submitted to *Solid State Nucl. Magn. Reson. pNMR Special Edition.*

Abstract

NMR spectroscopy of paramagnetic materials (pNMR) has the potential to provide great structural insight, but many challenges remain in interpreting the spectra in detail. This work presents a study of a series of structurally analogous metal-organic frameworks (MOFs) based on 5-substituted isophthalate linkers and Cu(II) paddlewheel dimers, of interest owing to their "crumple zone" structural rearrangement on dehydration/rehydration. ^{13}C MAS NMR spectra of the MOFs reveal a wide variation in the observed resonance position for chemically similar C species in the different MOFs but, despite this, resonances are overlapped in several cases. However, by considering a combination of the integration of quantitative spectra, the resonance position as a function of temperature and T_1 relaxation measurements, the spectra can be fully assigned. It is also demonstrated that the prototypical MOF in this series, STAM-1, displays a similar crumple zone rearrangement on dehydration to the well-characterised 5-ethoxyisophthalate MOF (STAM-17-OEt) although, while the materials have similar local C environments, dehydrated STAM-1 exhibits less long-range order.

Keywords: paramagnetic NMR, metal-organic frameworks, ^{13}C, fast magic angle spinning, Cu(II), paddlewheel dimer.

Introduction

Metal-organic frameworks (MOFs) are porous framework materials comprising an infinitely-connected network of metal ions or clusters connected by organic "linkers". MOFs are typically of great interest owing to their high porosity and the wide range of chemical space that they can cover. In particular, their crystal-chemical stability allows for the concept of isoreticularity, whereby the same framework topology can form with multiple different linkers or metals. This provides great potential to tune the physical and chemical properties of a MOF for specific applications in fields such as catalysis, guest storage and drug delivery.[1-3]

Many MOFs are unstable to hydrolysis, a phenomenon that Morris and co-workers have been seeking to address with hemilabile Cu(II)-based MOFs, containing copper "paddlewheel" dimers (Figure 1a) connected by 5-substituted isophthalate linkers (Figure 1b).[4,5] The archetypal material in this series is STAM-1, with a carboxymethyl substituent on the linker (Figure 1c).[4] The crystal structure of STAM-1 is shown in Figure 1d, and contains both hydrophobic pores (lined with the methyl ester groups) and hydrophilic pores (lined with Cu-bound water in the as-made material). Subsequently, McHugh *et al.*[5] prepared the isoreticular STAM-17-OEt, containing 5-ethoxyisophthalate linkers, and demonstrated that this material exhibited high hydrolytic stability, especially when compared to the more commonly used copper paddlewheel MOF, HKUST-1[6], containing benzene 1,3,5-tricarboxylate linkers (although it should be noted that Giovine *et al.*[7] recently demonstrated that HKUST-1 is surprisingly stable to steaming at 150-200 °C). The origin of this high hydrothermal stability was shown to be a rearrangement of the coordination environment of one half of the paddlewheel dimers upon dehydration, whereby the carboxylate oxygens of one dimer interact with the vacated axial site on the copper atoms of dimers above and below. This interaction requires energy to break, revealing the water coordination site on the copper atoms, and was described as being similar to the crumple zone of a car, in that the otherwise destructive impact of the incoming water molecules is dissipated in returning the MOF to its original state, rather than resulting in hydrolysis.[8]

The host-guest interactions in STAM-1 and STAM-17-OEt are fundamental to their rather unusual behaviour, and solid-state NMR spectroscopy has been demonstrated to be an excellent probe of structural changes, including host-guest interactions, on the local level (even when the material may be disordered on the long-range scale to which Bragg diffraction is sensitive).[9-12] However, many MOFs pose a challenge for NMR spectroscopy owing to the presence of paramagnetic metal cations and, even when the metal is diamagnetic, acquiring NMR spectra of many of the metals used can be very challenging.[11] It has previously been demonstrated that one of the simplest methods of enhancing resolution in NMR spectra of paramagnetic solids is to use very rapid magic angle spinning (MAS),[13-15] and this approach has previously been applied to obtain high-resolution ^{13}C MAS NMR spectra of copper paddlewheel-based MOFs.[16-18] Dawson *et al*. carried out a detailed ^{13}C NMR characterisation of as-made STAM-1 and observed the seven resonances expected by symmetry, albeit over the wide shift range of between *ca*. 850 and –50 ppm (Figure 1e).[18] By selective ^{13}C labelling of the linker and comparison with HKUST-1 (which can be considered as structurally analogous on the local level) it was shown that the resonance at the highest shift corresponded not to the carbon site closest to the Cu paddlewheel dimers (as might have been expected), but actually to the adjacent quaternary carbon, C1. The complete spectral assignment is shown in Figure 1e and further details can be found in Ref. [18].

This work presents the ^{13}C MAS NMR spectra of a series of Cu(II) isophthalate MOFs[5,19,20] and investigates the sensitivity of ^{13}C NMR spectroscopy to substitutions on the 5 position of the linker. It is also demonstrated that, although less ordered, the structure of dehydrated STAM-1 is very similar to that of dehydrated STAM-17-OEt on the local scale, confirming that this archetypal MOF also exhibits this interesting "crumple zone" response.

Methods

Synthesis

HKUST-1 was synthesised as previously reported.[18] $Cu(NO_3)_2.3(H_2O)$, (15.752 g, 66 mmol) and trimesic acid (9.262 g, 44 mmol) were dissolved in 264 mL EtOH/H_2O (50:50), stirred to homogeneity at room temperature, and heated at 110 °C for 1 day in a Teflon-lined steel autoclave. The autoclave was cooled to room temperature and HKUST-1 was isolated as a bright blue powder by suction filtration.

STAM-1 was synthesised as previously reported.[4,18] $Cu(NO_3)_2.3(H_2O)$ (0.991 g, 4.1 mmol) and trimesic acid (0.862 g, 4.1 mmol) were mixed with 20 mL MeOH/H_2O (50:50), stirred for 15 min at room temperature and then heated at 110 °C for 7 days in a Teflon-lined steel autoclave. The autoclave was cooled to room temperature, and large blue crystals were isolated by suction filtration and dried in air at 40 °C overnight.

STAM-17-Me was prepared by sonicating a suspension of 5-methyl isophthalic acid (180 mg, 1.0 mmol) and $Cu(OAc)_2.H_2O$ (200 mg, 1.0 mmol) in water (5 mL) and methanol (10 mL) for 3 minutes. The mixture was then sealed in a Teflon-lined steel autoclave and heated to 110 °C for three days. Upon cooling to room temperature, filtering and drying under air at 40 °C overnight, STAM-17-Me was collected as a blue powder (253 mg, 0.97 mmol, 98% yield). Elemental analysis Calcd for $CuC_9H_8O_5 \cdot H_2O$ C: 38.92 H: 3.63, Found C: 39.01 H: 3.28%.

STAM-17-OMe was prepared by heating a suspension of $Cu(OAc)_2.H_2O$ (201 mg, 1.0 mmol) and 5-methoxy isophthalic acid (196 mg, 1.0 mmol) in water (5 mL) and ethanol (10 mL) to 110 °C in a Teflon-lined steel autoclave for three days. Upon cooling to room temperature, filtering and drying under air at 40 °C overnight, STAM-17-OMe was isolated as a blue crystalline solid (227 mg, 0.82 mmol, 82% yield). Elemental analysis Calcd for $CuC_9H_8O_6 \cdot 0.5H_2O$ C: 37.97 H: 3.19, Found C: 37.83 H: 3.14%.

The other members of the STAM-17 series were synthesised as previously reported.[5] Using STAM-17-OEt as an example, the material was synthesised by heating $Cu(OAc)_2.H_2O$ (0.20 g, 1.00 mmol), 5-ethoxyisophthalic acid (0.21 g, 1.00 mmol) and distilled water (15 mL) were heated in a Teflon-lined autoclave at 110 °C for 3 days. Upon cooling to room temperature, filtering and drying under air at 40 °C overnight, the blue products were obtained in typical yields of 80-95% (based on the mass of linker). STAM-17-O^{n}Pr and STAM-17-O^{n}Bu were prepared in the same way from the corresponding

linker. All samples were used as made, except for STAM-17-O^{i}Bu, which was evacuated at 150 °C overnight to remove residual ethanol from washing, and then rehydrated by exposure to air prior to spectral acquisition. Scheme 1 shows the linkers present in the STAM-17 series and the numbering scheme used throughout this work.

Solid-state NMR spectroscopy

Solid-state NMR spectra were acquired using Bruker Avance III spectrometers equipped with 9.4 or 14.1 T wide-bore superconducting magnets. For magic angle spinning (MAS) spectra, samples were packed into zirconia rotors with an outer diameter of 1.9 mm and rotated at rates of up to 40 kHz (9.4T) or zirconia rotors with an outer diameter of 1.3 mm and rotated at rates of up to 60 kHz (14.1 T). Spectra were acquired using a rotor-synchronised spin-echo sequence, with an echo interval of one rotor period (*i.e.*, between 16.7 and 26.7 μs). A radiofrequency field strength of ν_1 = 125 kHz was used for all experiments. The longitudinal relaxation constants, T_1, were measured using inversion recovery experiments and analysed using the Dynamics Centre in TopSpin 3.5.6 (Bruker). Isotropic peak positions, δ_{iso}, and apparent transverse relaxation constants, T_2*, were measured using DMFIT.[21] In all cases, the sample temperature was controlled using a Bruker BCU-II chiller and BVT/BVTB 3000 temperature controller and heater booster. The sample temperature was calibrated for the MAS rates employed using the temperature-dependent ^{87}Rb shift of RbCl.[22] Chemical shifts are reported in ppm relative to tetramethylsilane using the CH_3 resonance of L-alanine (δ = 20.5 ppm) as a secondary reference. Further experimental details are given in the ESI.

Results and Discussion

Acquisition and assignment of ^{13}C NMR spectra of STAM-17 analogues

The ^{13}C MAS NMR spectrum of STAM-1 (shown above in Figure 1 for the as-made material) spans the range from almost 1000 to –150 ppm.[18,23-25] However, to acquire the entire spectrum without distortion, frequency stepping of the transmitter is required, as well as extensive signal averaging. The only benefit of the lengthy frequency-stepping

process is the observation of the C1 resonance between 700 and 900 ppm. This resonance is very broad relative to its temperature- and chemistry-dependent shift range and, as such, the effort expended in observing it can generally be more usefully spent on other experiments. Therefore, for the remainder of this work, we focus our attention on the more readily-observed region between 300 and –150 ppm in the analogues of STAM-17. For completeness, spectra exhibiting the C1 resonances were recorded (using more rapid 60 kHz MAS and the higher field of 14.1 T to improve the sensitivity of the rotor-synchronised spin-echo experiment to the observation of very broad resonances) and are shown in the ESI. However, no temperature-dependent measurements were recorded for C1 in any of the STAM-17 materials discussed below.

STAM-17-Me

Figure 2 shows variable-temperature (VT) ^{13}C MAS NMR spectra of STAM-17-Me. Four resonances are observed at all temperatures, with shifts between 230 and –65 ppm. This is fewer than the expected five resonances one would expect for C2-C6 (C1 was observed at ~770 ppm at 298 K, see ESI). Truly quantitative pNMR spectra are very challenging to record, particularly in copper paddlewheel dimer MOFs where there is a wide range of longitudinal and transverse relaxation rates across the material. Table 1 reports longitudinal (T_1) and apparent transverse (T_2*) relaxation time constants at 298 K for the four resonances observed (see ESI for further details). The relaxation interval of 100 ms chosen for these experiments is greater than 5 T_1 for the resonance with the slowest longitudinal relaxation and the rotor-synchronised spin-echo delay of 26.7 μs is small relative to the T_2* values, suggesting that the spectra shown in Figure 2 are at least pseudo-quantitative. At 298 K the relative integrated intensity ratios of the resonances observed at 221.3, 179.3, 24.8 and –60.3 ppm for STAM-17-Me are 1.0 : 3.1 : 1.3 : 1.6, suggesting that (if the resonance at 221.3 ppm corresponds to C3, as might be expected from earlier work for STAM-1[18]) the resonance at 179.3 ppm corresponds to an overlap of resonances from C4 (crystallographically-expected relative intensity of 2) and C5 (expected relative intensity of 1). It can be seen from the VT ^{13}C MAS NMR spectra of STAM-17-Me (Figure 2) that the resonances from C4 and C5 are completely overlapped

over the temperature range studied, indicating that both species have a very similar (and relatively small) interaction with the unpaired electrons. The broad (~3 kHz) resonance at –60.4 ppm can be assigned to C2 by comparison with STAM-1 and HKUST-1,[18] and the resonance at 24.8 ppm can, thus, be assigned to C6. Note that, owing to signal loss from relaxation effects (see Table 1), the relative intensities of C6 (expected relative intensity of 1, observed 1.3) and C2 (expected 2, observed 1.6) are over- and under-estimated, respectively, relative to the signal for C3.

For a simple mononuclear Cu(II) complex, a plot of δ_{iso} against 1/T would be linear with a gradient directly related to the electron-nuclear hyperfine coupling constant and an intercept corresponding to the diamagnetic orbital shift contribution (*i.e.*, the "chemical shift" contribution) to δ_{iso}.[26,27] However, in the presence of a copper paddlewheel dimer (S = 1) there exists a diamagnetic open-shell singlet ground state and a paramagnetic triplet excited state. The triplet state contributes to a paramagnetic shift and, crucially, will be populated at infinite temperature, leading to a paramagnetic contribution to the y-intercept. Furthermore, the shape of the plot will have contributions from both the magnitude of the hyperfine coupling constant and the varying thermal population of the triplet state. Campbell and Haw[28] estimated the temperature-dependent shift of a resonance affected only by the hyperfine coupling (*i.e.* a simple binuclear copper paddlewheel complex) as

$$\nu_{obs} = \nu_{dia} + \nu_0 \frac{2g\mu_B A}{(\gamma_C/2\pi)kT} \cdot \frac{1}{3+e^{2J/kT}} \quad , \qquad (1)$$

where ν_{obs} is the observed frequency, ν_{dia} is the diamagnetic contribution, ν_0 is the Larmor frequency, g is the electronic g factor, μ_B is the Bohr magneton, A is the hyperfine coupling constant in MHz, γ_C is the gyromagnetic ratio for ^{13}C, k is the Boltzmann constant, T is the absolute temperature and 2J is the singlet-triplet splitting (note that J is quoted as a negative number as the singlet is lower in energy than the triplet). However, in an infinitely-connected MOF, the electronic structure becomes yet more complicated, with each linker connected to multiple paddlewheel dimers. From SQUID magnetometry measurements of STAM-1, Mohideen *et al.* determined the presence of an antiferromagnetic coupling of –308(1) cm^{-1} and a ferromagnetic (*i.e.*, inter-dimer) coupling

of 107(2) cm^{-1}.[29,30] Additionally, a significant dipolar contribution (with a range of several nm[31,32]) may also be expected to affect the NMR spectrum. This prevents the ready extraction of accurate values of A and J from the VT NMR spectra presented here. In order to experimentally obtain such parameters from solid-state NMR spectra of these MOFs, a much wider temperature range would need to be accessed, which is not possible with the currently available hardware, while maintaining the rapid MAS rates used. However, work is ongoing[33] to adapt the computational methodology we have introduced to predict pNMR parameters for mononuclear complexes[26,27] to the more challenging systems of infinitely-connected copper paddlewheel MOFs.

STAM-17-OR (R = Me, Et, ^{n}Pr, ^{n}Bu, ^{i}Bu)

Figure 3 shows the VT ^{13}C MAS NMR spectra of STAM-17-OMe. At 298 K, the number of resonances observed is not consistent with the structure of the linker. Measurement of T_1 and T_2* time constants (see Table 2) for each resonance again indicated that the spectrum should be pseudo-quantitative and the relative spectral intensities of 1.8 : 1.8 : 1.0 : 1.3 indicated that, in this case, the C5 resonance now overlaps with the C3 resonance at 218 ppm, rather than with the C4 resonance as observed for STAM-17-Me. At 298 K the resonance can, indeed, be decomposed into two Lorentzian contributions with relative integrals of 1.5 and 1.0 and isotropic shifts of 218.7 and 216.4 ppm, suggesting their assignment as C5 and C3, respectively (since C3 might be expected to experience a greater loss of signal during the spin echo than C5, owing to the smaller T_2* of the former). As shown in the expansions in Figure 3, the C3 and C5 resonances become more clearly separated at higher temperatures (as previously reported for STAM-17-OEt[5]). While it is, perhaps, surprising that C5 has a higher isotropic shift than C3 (under the temperature range investigated here), the position of the resonance assigned to C3 varies more with temperature, indicating that it arises from a C species with a shorter through-bond pathway to Cu (*i.e.*, a larger hyperfine coupling constant). This assignment is also consistent with that for the other 5-alkoxyisophthalate MOFs discussed below. The remaining three resonances can be identified as C2 (–57.4 ppm), C4 (165.7 ppm) and C6

(50.0 ppm) by their isotropic shifts, temperature dependences and T_1 relaxation constants (see Table 2).

The ^{13}C MAS NMR spectra of the other alkoxy derivatives (*i.e.*, STAM-17-OR (R = Et, ^{n}Pr, ^{n}Bu, ^{i}Bu), shown in Figure 4a, are very similar to that of STAM-17-OMe, with the C3 and C5 resonances very close at room temperature. However, as shown by the inset in Figure 4a, the separation between these two resonances at 298 K increases with increasing alkyl chain length, such that for the propoxyl- and butoxyl-based MOFs, the resonances are clearly resolved. As shown in Figure 4b, this change in the separation of C3 and C5 resonances cannot be explained by either C3 or C5 alone moving systematically to higher or lower shift with increasing chain length. As for STAM-17-OMe, the C3 and C5 resonances for the other alkoxy MOFs all separate more at high temperature, with C3 exhibiting a greater shift difference than C5 (see the ESI for VT ^{13}C NMR spectra and pNMR parameters for these MOFs).

STAM-1

The ^{13}C MAS NMR spectrum of STAM-1 has already been reported by Dawson *et al*.[18] and was also shown in Figure 1d. For this work, the ^{13}C pNMR parameters and VT NMR spectra for this MOF were recorded under the same conditions as those used for the other members of the STAM-17 family, allowing direct comparison of the values obtained. Figure 5 shows the VT ^{13}C NMR spectra of STAM-1, along with the assignment from Ref. [18] and Table 3 reports the relaxation constants, T_1 and T_2*.

Several trends can be observed in the ^{13}C NMR spectra of the MOFs studied here. In general, the C1 resonance is very broad and appears at very high shift, the C2 resonance is also broadened and appears at *ca*. –50 to –60 ppm, and the C3 resonance is relatively sharp and occurs at *ca*. 216-227 ppm. Despite C3 and C4 being the same number of bonds (and a very similar distance) away from the Cu centres, the shift of C4 is much more sensitive to the nature of the substituent on the linker, exhibiting a range of ~15 ppm. Perhaps unsurprisingly, the shift of C5 is even more sensitive to the nature of the attached substituent, with a shift range of ~45 ppm. These trends can be explained by the relative strength of electron donation of the substituents with OR > R > CO_2R, such that C5 will be

more electron rich and, hence will have more electron density with which to interact with the unpaired spin, leading to a larger paramagnetic shift. In addition to this electronic effect, there is likely a steric effect, owing to the different physical bulk of the 5-substituents. This steric contribution is likely to account for at least some of the non-linearity of the variation in C3 and C5 δ_{iso} observed in Figure 4b. It is, however, worth noting that, despite the wide variation in observed δ_{iso} for the chemically analogous sites in the different MOFs, the T_1 relaxation constants are very similar, as seen in Figure 6. From this plot, it can also be seen that T_1 increases systematically the further away a C atom is from the paramagnetic centre, suggesting that T_1 measurements may be a more reliable parameter to use in assignments than δ_{iso}. (It should be noted that T_1 values for C1 were not measured for this work but the previous work of Dawson *et al.*[18] indicates that, T_1 for C1 and C2 is very similar to within experimental error, although C1 perhaps exhibits slightly more rapid relaxation).

The nuclear T_1 is strongly influenced by the electron-nuclear dipolar interaction,[32] and one might expect a more reliable correlation to be achieved by considering (as in the work of Brough *et al.*[31]) interactions with all paramagnetic centres within tens of Å. However, for these MOFs, the paramagnetic species is the ferromagnetically-coupled triplet state of the paddlewheel dimer (with a Cu-Cu separation of ~2.6 Å), which cannot be treated as a simple point dipole, and Ke *et al.*[33] have computed significant spin delocalisation onto the linker for the model $Cu_2(CO_2C_6H_5)_4.2$(urea) system, which further complicates such detailed analysis. However, since the dimers are fairly sparse in the MOFs and the spin delocalisation is likely to be quite similar to the model case, the proxy of the number of bonds to the nearest dimer, as used in Figure 6, is a reasonable parameter for capturing both the proximity of the nearest paramagnetic metallic centres and also the extent of spin delocalisation on nearby atoms.

Dehydration of STAM-1 and STAM-17-OEt

In addition to containing both hydrophilic and hydrophobic (or otherwise functionalisable) pores within the same MOF, the STAM-17 family is of interest owing to

the high hydrolytic stability of the dehydrated materials (compared to HKUST-1, which has a similar local structure).[5] For STAM-17-OEt, McHugh *et al*.[5] demonstrated that this stability arises from the ability of the framework to reversibly rearrange upon dehydration, leading to an interaction between the carboxylate O atom of one paddlewheel unit and the axial position of a Cu on the dimer above or below, as shown in Figure 7a. Upon rehydration of the MOF, the framework rearrangement must be reversed, and this absorbs some of the energy of the incoming water molecule and provides additional stability by preventing hydrolysis of the equatorial Cu-carboxylate bonds. To facilitate this structural rearrangement, half of the paddlewheel dimers of the dehydrated MOF must adopt the alternative arrangement, shown in Figure 7b, where there is no axial Cu-O interaction. This leads to a lowering of the symmetry and the presence of four crystallographically independent linker species. Consequently, the ^{13}C MAS NMR spectrum of dehydrated STAM-17-OEt, shown in Figure 7c, contains multiple overlapping resonances. By using ^{1}H-^{13}C cross-polarisation (CP) experiments,[5,34] the spectrum could be assigned as shown in Figure 7c.

Since the initial synthesis of STAM-1, it has been known that dehydration of the MOF leads to a lowering of symmetry.[4,29] However, the structure of the dehydrated MOF has not been determined in detail owing to low-quality diffraction data, which suggested a loss of crystalline order.[4,29] The ^{13}C MAS NMR spectrum of dehydrated STAM-1 is shown in Figure 7d and was first reported by Dawson *et al*.[18] but not assigned. By comparison with the ^{13}C MAS NMR spectrum of dehydrated STAM-17-OEt in Figure 7c, it can be seen that the structure of dehydrated STAM-1 is likely to be very similar on a local level (leading to similar isotropic shifts, particularly for C2), but with less long-range order leading to a broadening of the resonances. This observation confirms that the "crumple zone" rehydration mechanism of STAM-1 is, on the atomic scale, very similar to that for STAM-17. For comparison, despite the very similar local structure, HKUST-1 does not undergo a framework rearrangement upon dehydration (although the two Cu atoms within the dimer have been shown to move slightly closer to each other[6]) and there are no axial Cu-O interactions. This leads to only a single resonance being observed for C2, at –87 ppm, as shown in Figure 7e. Therefore, the resonances between 0

and –65 ppm for dehydrated STAM-1 and STAM-17-OEt can initially be assigned to C2 in dimers with axial Cu-O interactions (reminiscent of the hydrated structure) and the resonances between –65 and –110 ppm to C2 in dimers without such axial interactions (*cf.* HKUST-1). However, the C2 region of the ^{13}C MAS NMR spectrum of dehydrated STAM-17-OEt can be decomposed into five resonances with shifts (at 298 K) of –7.8, –30.6, –48.8, –93.6 and –102.3 ppm, with relative integrated intensities of 1 : 1 : 1 : 1 : 2. From the crystal structure, one would, indeed, expect six types of C2 with equal populations, but four of these belong to dimers with axial Cu-O interactions, whereas only two belong to dimers without these interactions. The detailed assignment of these resonances, therefore, appears more complex than might initially be assumed, and, from the integrated intensities, it can be suggested that the resonance at –93.6 ppm must also arise from a C2 species in a dimer with an axial Cu-O interaction.

Conclusions

This study has extended our initial work on Cu(II) paddlewheel crumple zone MOFs and investigates the effect of linker variation on their high-resolution ^{13}C MAS NMR spectra. We have demonstrated that, by using rapid MAS, it is possible to record an essentially quantitative ^{13}C NMR spectrum of these materials on a reasonable timescale, although this omits the C1 resonance, which is typically found at much higher shift and it much broader than the other resonances. The acquisition of quantitative spectra is essential to spectral assignment as, in both the alkyl and alkoxy forms of STAM-17, the C5 resonance overlaps (completely or partially) with another resonance. The C5 shift appears to be related to the electron donating ability of the substituent on the linker, with strongly-donating substituents (OR) leading to higher shifts and the electron withdrawing CO_2R substituent leading to a shift that is ~45 ppm lower.

Despite the unreliability of assigning spectra based purely on isotropic shifts, it was shown that (with the exception of C1) the T_1 relaxation constant provides a reliable indication of the distance from the nucleus to the paramagnetic centre, with little variation with the chemical nature of the linker. This parameter may, therefore, be of use in future

characterisation of families of paramagnetic MOFs, where the spectral assignment is unknown.

The sensitivity of solid-state NMR spectroscopy to structure on the local scale was also used to provide insight into the structure of dehydrated STAM-1. This material was known to undergo some form of reversible structural rearrangement on dehydration and it was shown that, although exhibiting less long-range order than dehydrated STAM-17-OEt (for which the crystal structure has been determined[5]), the structure of dehydrated STAM-1 is very similar to that of dehydrated STAM-17-OEt on the local scale, suggesting a similar crumple zone behaviour is exhibited.

Acknowledgements

SEA thanks the Royal Society and Wolfson Foundation for a merit award. REM and LNM thank the EPSRC for support (EP/N50936X/1). The research data (and/or materials) supporting this publication can be accessed at DOI: 10.17630/0c27a0c9-aa47-47e4-b30a-a215976c3dbe.[35]

References

[1] K. Sumida, D.L. Rogow, J.A. Mason, T.M. McDonald, E.D. Bloch, Z.R. Herm, T.-H. Bae, J.R. Long, Carbon Dioxide Capture in Metal-Organic Frameworks. Chem. Rev. 112 (2012) 724–781. DOI: 10.1021/cr2003272.

[2] M.P. Suh, H.J. Park, T.K. Prasad, D.W. Lim, Hydrogen Storage in Metal-Organic Frameworks. Chem. Rev. 112 (2012) 782–835. DOI: 10.1021/cr200274s.

[3] A.C. McKinlay, R.E. Morris, P. Horcajada, G. Férey, R. Gref, P. Couvreur, C. Serre, BioMOFs: Metal-Organic Frameworks for Biological and Medical Applications. Angew. Chem. Int. Ed. 49 (2010) 6260–6266. DOI: 10.1002/anie.201000048.

[4] M.I.H. Mohideen, B. Xiao, P.S. Wheatley, A.C. McKinlay, Y. Li, A.M.Z. Slawin, D.W. Aldous, N.F. Cessford, T. Düren, X. Zhao, R. Gill, K.M. Thomas, J.M. Griffin, S.E. Ashbrook, R.E. Morris, Protecting Group and Switchable Pore-Discriminating Adsorption Properties of a Hydrophilic–Hydrophobic Metal–Organic Framework. Nature Chem. 3 (2011) 304–310. DOI: 10.1038/nchem.1003.

[5] L.N. McHugh, M.J. McPherson, L.J. McCormick, S.A. Morris, P.S. Wheatley, S.J. Teat, D. McKay, D.M. Dawson, C.E.F. Sansome, S.E. Ashbrook, C.A. Stone, M.W. Smith, R.E. Morris, Hemilability Increases Hydrolytic Stability in Metal-Organic Frameworks. Nature Chem. 10 (2018) 1096–1102. DOI: 10.1038/s41557-018-0104-x.

[6] S.S.-Y. Chui, S.M.-F. Lo, J.P.H. Charmant, A.G. Orpen, I.D. Williams, Chemically Functionalizable Nanoporous Material $[Cu_3(TMA)_2(H_2O)_3]_n$. Science 283 (1999) 1148–1149. DOI: 10.1126/science.283.5405.1148.

[7] R. Giovine, F. Pourpoint, S. Duval, O. Lafon, J.-P. Amoureux, T. Loiseau, C. Volkringer, The Surprising Stability of $Cu_3(btc)_2$ Metal−Organic Framework under Steam Flow at High Temperature. Cryst. Growth Des. 18 (2018) 668–6693. DOI: 10.1021/acs.cgd.8b00931.

[8] J. Senker, Crumple Zones in MOFs. Nature Chem. 10 (2018) 1079–1081. DOI: 10.1038/s41557-018-0161-1.

[9] S.E. Ashbrook, D.M. Dawson, V.R. Seymour, Recent Developments in Solid-State NMR Spectroscopy of Crystalline Microporous Materials. Phys. Chem. Chem. Phys. 16 (2014) 8223–5242. DOI: 10.1039/c4cp00578c.

[10] R.F. Moran, D.M. Dawson, S.E. Ashbrook, Exploiting NMR Spectroscopy for the Study of Disorder in Solids. Int. Rev. Phys. Chem. 36 (2017) 39–115. DOI: 10.1080/0144235x.2017.1256604.

[11] P. He, B.E.G. Lucier, V.V. Terskikh, Q. Shi, J. Dong, Y. Chu, A. Zheng, A. Sutrisno, Y. Huang, Spies within Metal-Organic Frameworks: Investigating Metal Centers using Solid-State NMR. J. Phys. Chem. C 118 (2014) 23728–23744. DOI: 10.1021/jp5063868.

[12] B.E.G. Lucier, S. Chen, Y. Huang, Characterization of Metal–Organic Frameworks: Unlocking the Potential of Solid-State NMR. Acc. Chem. Res. 51 (2018) 319–330. DOI: 10.1021/acs.accounts.7b00357.

[13] Y. Ishii, N.P. Wickramasinghe, S. Chimon, A New Approach in 1D and 2D ^{13}C High-Resolution Solid-State NMR Spectroscopy of Paramagnetic Organometallic Complexes by Very Fast Magic-Angle Spinning. J. Am. Chem. Soc. 125 (2003) 3438–3439. DOI: 10.1021/ja0291742.

[14] N.P. Wickramasinghe, Y. Ishii, Sensitivity Enhancement, Assignment, and Distance Measurement in ^{13}C Solid-State NMR Spectroscopy for Paramagnetic Systems under Fast Magic Angle Spinning. J. Magn. Reson. 181 (2006) 233–243. DOI: 10.1016/j.jmr.2006.05.008.

[15] I. Bertini, L. Emsley, M. Lelli, C. Luchinat, J. Mao, G. Pintacuda, Ultrafast MAS Solid-State NMR Permits Extensive ^{13}C and ^{1}H Detection in Paramagnetic Metalloproteins. J. Am. Chem. Soc. 132 (2010) 5558–5559. DOI: 10.1021/ja100398q.

[16] G.W. Peterson, G.W. Wagner, A. Balboa, J. Mahle, T. Sewell, C.J. Karwacki, Ammonia Vapor Removal by $Cu_3(BTC)_2$ and its Characterization by MAS NMR. J. Phys. Chem. C 113 (2009) 13906–13917. DOI: 10.1021/jp902736z.

[17] F. Gul-E-Noor, B. Jee, A. Pöppl, M. Hartmann, D. Himsl, M. Bertmer, Effects of Varying Water Adsorption on a $Cu_3(BTC)_2$ Metal–Organic Framework (MOF) as Studied by ^{1}H and ^{13}C Solid-State NMR Spectroscopy. Phys. Chem. Chem. Phys. 13 (2011) 7783–7788. DOI: 10.1039/c0cp02848g.

[18] D.M. Dawson, L.E. Jamieson, M.I.H. Mohideen, A.C. McKinlay, I.A. Smellie, R. Cadou, N.S. Keddie, R.E. Morris, S.E. Ashbrook, High-Resolution Solid-State ^{13}C NMR Spectroscopy of the Paramagnetic Metal–Organic Frameworks, STAM-1 and HKUST-1. Phys. Chem. Chem. Phys. 15 (2013) 919–929. DOI: 10.1039/c2cp43445h.

[19] B. Garai, A. Mallick, A. Das, R. Mukherjee, R. Banerjee, Self-Exfoliated Metal-Organic Nanosheets through Hydrolytic Unfolding of Metal-Organic Polyhedra. Chem. Eur. J. 23 (2017) 7361–7366. DOI: 10.1002/chem.201700848.

[20] O. Barreda, G. Bannwart, G.P.A. Yap, E.D. Bloch, Ligand-Based Phase Control in Porous Molecular Assemblies. ACS Appl. Mater. Interfaces 10 (2018) 11420–11424. DOI: 10.1021/acsami.8b02015.

[21] D. Massiot, F. Fayon, M. Capron, I. King, S. Le Calvé, B. Alonso, J.-O. Durand, B. Bujoli, Z. Gan, G. Hoatson, Modelling One- and Two-Dimensional Solid-State NMR Spectra. Magn. Reson. Chem. 40 (2002) 70–76. DOI: 10.1002/mrc.984.

[22] J. Skibsted, H.J. Jakobsen, Variable-Temperature ^{87}Rb Magic-Angle Spinning NMR Spectroscopy of Inorganic Rubidium Salts. J. Phys. Chem. A 103 (1999) 7958–7971. DOI: 10.1021/jp9912861.

[23] D.M. Dawson, Ph.D. Thesis, University of St Andrews (2014). URL: http://hdl.handle.net/10023/7053.

[24] L.E. Jamieson, MChem. Thesis, University of St Andrews (2012).

[25] H.L.B. Boström, MChem. Thesis, University of St Andrews (2014).

[26] M. Bühl, S.E. Ashbrook, D.M. Dawson, R.A. Doyle, P. Hrobárik, M. Kaupp, I.A. Smellie, Paramagnetic NMR of Phenolic Oxime Copper Complexes: a Joint Experimental and Density Functional Study. Chem. Eur. J. 22 (2016) 15328–15339. DOI: 10.1002/chem.201602567.

[27] D.M. Dawson, Z. Ke, F.M. Mack, R.A. Doyle, G.P.M. Bignami, I.A. Smellie, M. Bühl, S.E. Ashbrook, Calculation and Experimental Measurement of Paramagnetic NMR Parameters of Phenolic Oximate Cu(II) Complexes. Chem. Comm. 53 (2017) 10512–10215. DOI: 10.1039/c7cc05098d.

[28] G.C. Campbell, J.F. Haw, Determination of Magnetic and Structural Properties in Solids Containing Antiferromagnetically Coupled Metal Centers using NMR Methods. Magneto-Structural Correlations in Anhydrous Copper(II) *n*-Butyrate, Inorg. Chem. 27 (1988) 3706–3709. DOI: 10.1021/ic00294a007.

[29] M.I.H. Mohideen, Ph.D. Thesis, University of St Andrews (2011). URL: http://hdl.handle.net/10023/1892.

[30] H. El Mkami, M.I.H. Mohideen, C. Pal, A. McKinlay, O. Scheimann, R.E. Morris. EPR and Magnetic Studies of a Novel Copper Metal Organic Framework (STAM-1). Chem. Phys. Lett. 544 (2012) 17–21. DOI 10.1016/j.cplett.2012.06.012.

[31] A.R. Brough, C.P. Grey, C.M. Dobson, Paramagnetic Ions as Structural Probes in Solid-State NMR: Distance Measurements in Crystalline Lanthanide Acetates. J. Am. Chem. Soc. 115 (1993) 7318–7327. DOI: 10.1021/ja00069a034.

[32] A.J. Pell, G. Pintacuda, C.P. Grey, Paramagnetic NMR in Solution and the Solid State. Prog. Nucl. Magn. Reson. Spectrosc. 111 (2019) 1–271. DOI: 10.1016/j.pnmrs.2018.05.001.

[33] Z. Ke, L.E. Jamieson, D.M. Dawson, S.E. Ashbrook, M. Bühl, NMR chemical shifts of urea loaded copper benzoate. A joint solid-state NMR and DFT study. Solid State Nucl. Magn. Reson. In press. DOI: 10.1016/j.ssnmr.2019.04.004.

[34] C.E.F. Sansome, MChem Thesis, University of St Andrews (2016).

[35] D.M. Dawson, C.E.F. Sansome, L.N. McHugh, R.E. Morris, S. E. Ashbrook, ^{13}C pNMR of "Crumple Zone" Cu(II) Isophthalate Metal-Organic Frameworks (Dataset). University of St Andrews Research Portal. (2019). https://doi.org/10.17630/0c27a0c9-aa47-47e4-b30a-a215976c3dbe.

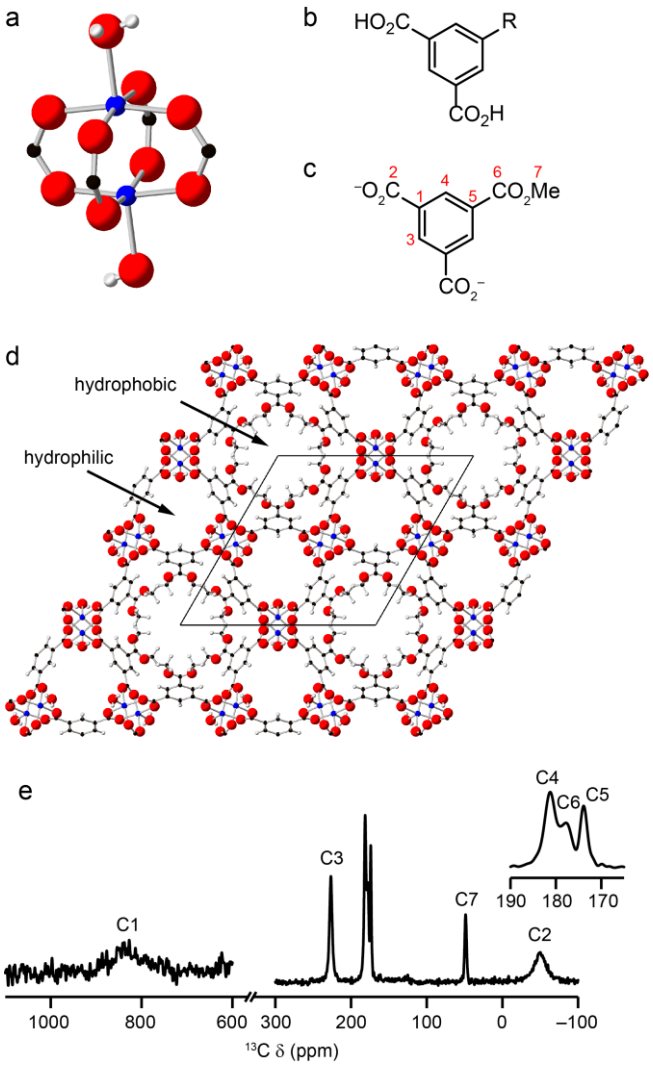

Figure 1. (a) Structure of a copper paddlewheel dimer – the axial ligands (here H_2O) are labile. Schematic structure of (b) a 5-substituted isophthalic acid and (c) the 5-carboxymethylisophthalate linker of STAM-1, along with (in red) the atomic numbering scheme used in this work. (d) Crystal structure of STAM-1[4] (H_2O in the hydrophobic pores are omitted for clarity). (e) ^{13}C (14.1 T, 60 kHz MAS, room temperature) NMR spectrum of STAM-1, with the assignment of Dawson *et al.*[18] indicated (note that the spectrum of C1 was recorded in a separate sub-spectrum and is shown processed with 200 Hz Lorentzian broadening). In (a) and (d), atoms are coloured Cu = blue, C = black, O = red, H = pale grey.

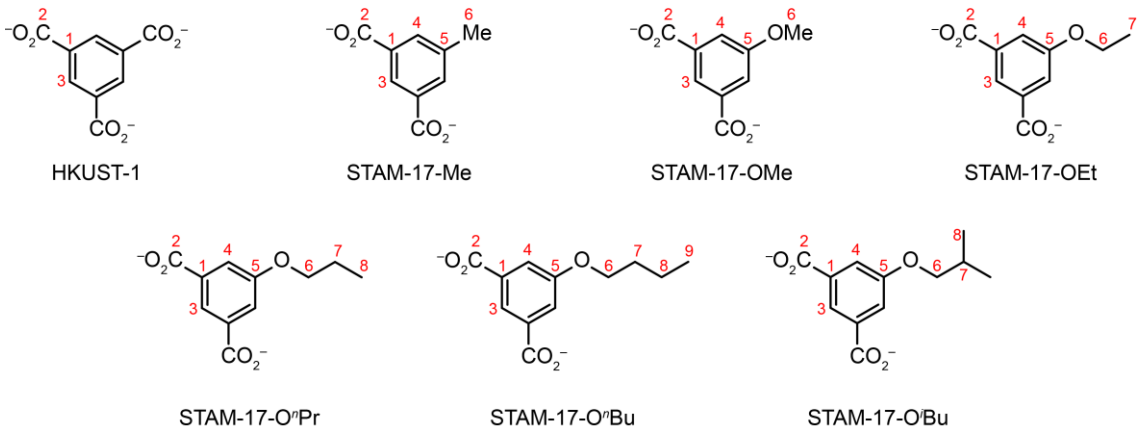

Scheme 1. Linkers used to prepare HKUST-1 and the STAM-17 series, with (in red) the numbering schemes used in this work.

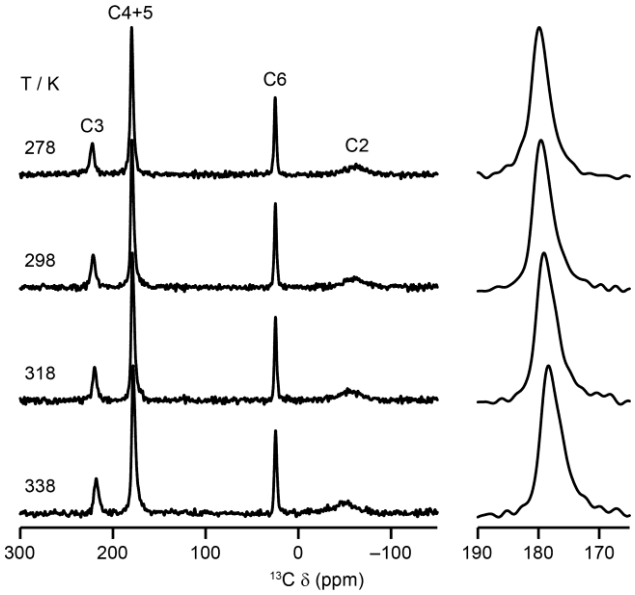

Figure 2. VT ^{13}C (9.4 T, 37.5 kHz MAS) NMR spectra of STAM-17-Me with the expansions showing the C4 + C5 region.

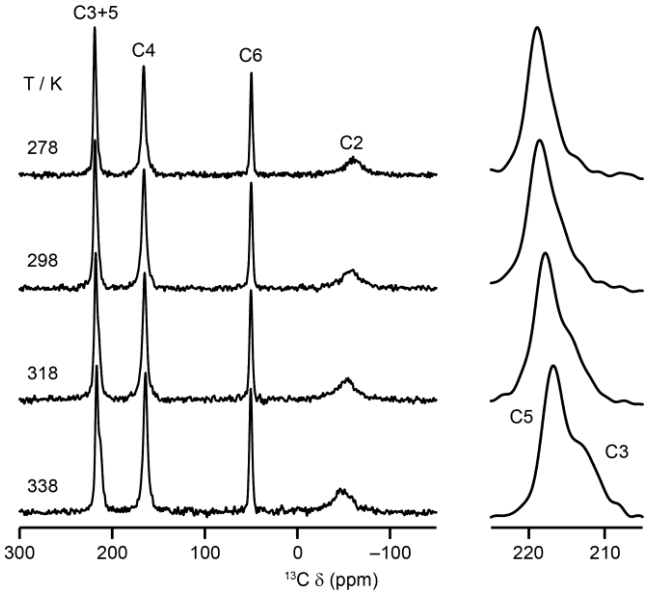

Figure 3. VT ^{13}C (9.4 T, 37.5 kHz MAS) NMR spectra of STAM-17-OMe, with the expansions showing the C3 + C5 region.

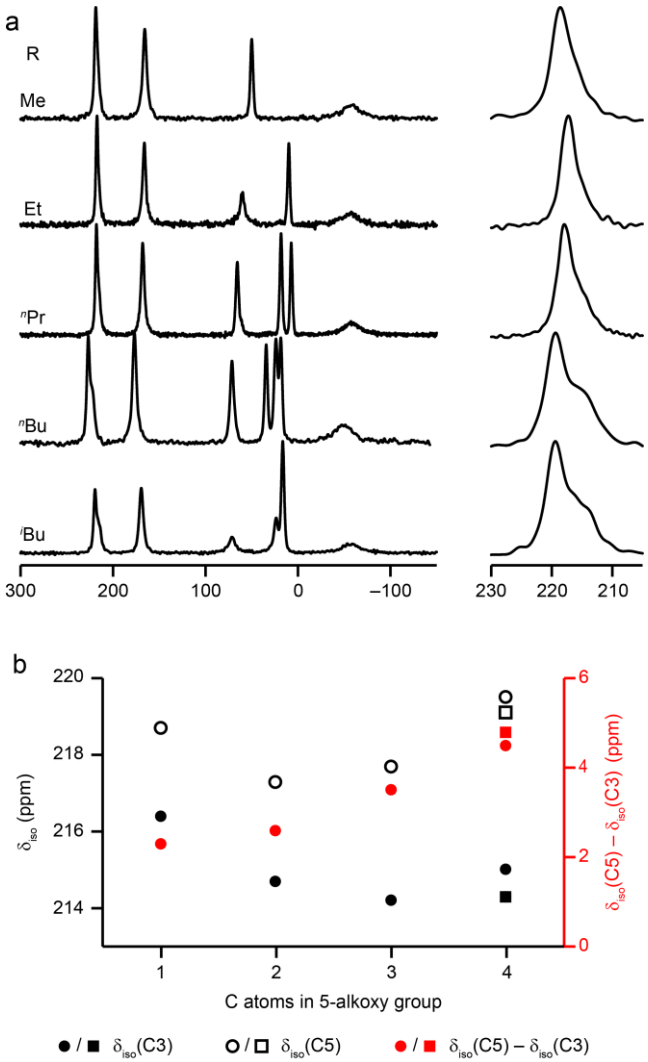

Figure 4. (a) ^{13}C (9.4 T, 37.5 kHz MAS, 298 K) NMR spectra of STAM-17-OR (R = Me, Et, ^{n}Pr, ^{n}Bu, ^{i}Bu) with the expansion showing the C3 + C5 region. (b) Plot of (left axis) the C3 and C5 δ_{iso} (at 298 K) of STAM-17-OR and (right axis) the C3 - C5 shift difference as a function of chain length. Points for STAM-17-O^{i}Bu are shown as squares.

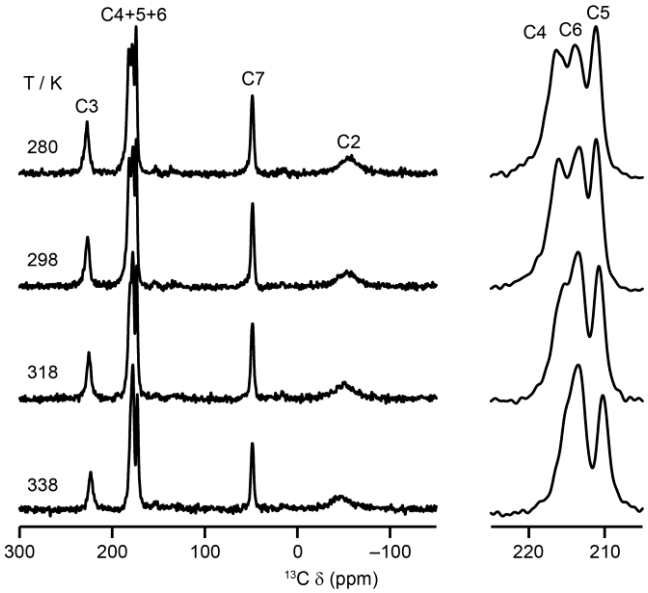

Figure 5. VT ^{13}C (9.4 T, 37.5 kHz MAS) NMR spectra of STAM-1 with the expansion showing the C4 + C5 + C6 region.

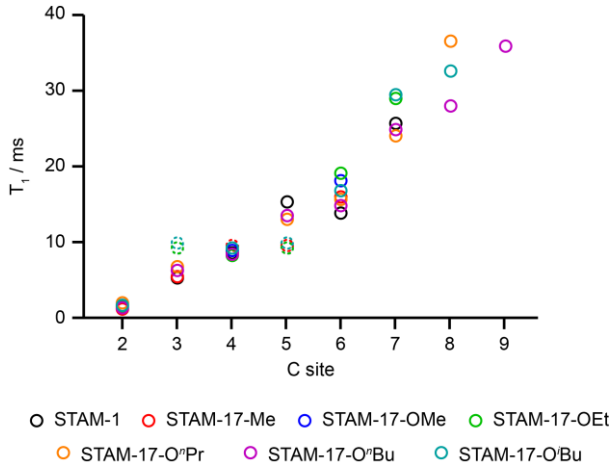

Figure 6. Plot of T_1 for the different C sites in STAM-1 and the STAM-17 variants studied here. Broken lines indicate points where two resonances overlap in the T_1 measurements (C4 + C5 in STAM-17-Me and C3 + C5 in STAM-17-OMe, STAM-17-OEt and STAM-17-O^{i}Bu).

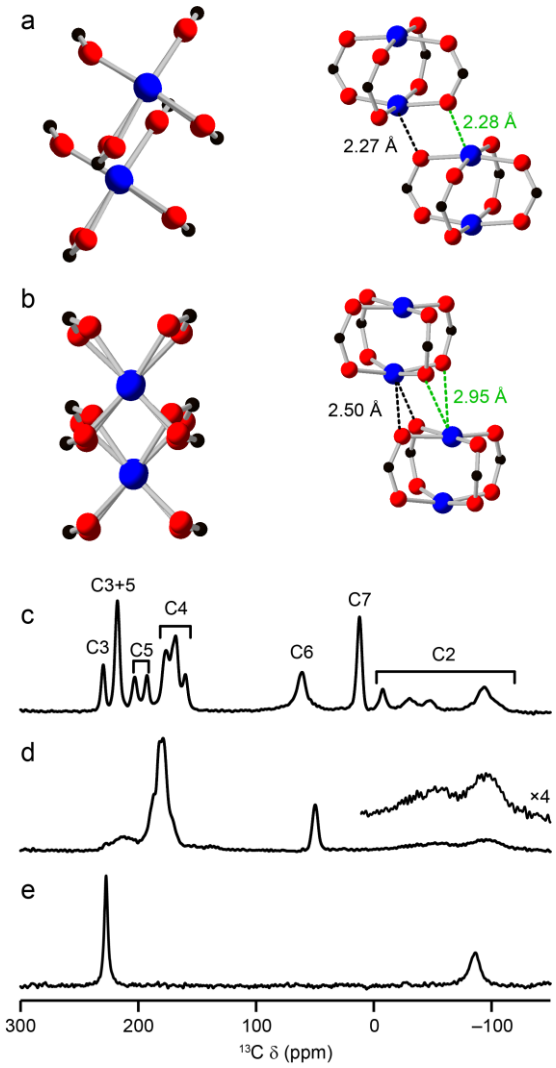

Figure 7. Local environments of the (a) Cu1-Cu2 and (b) Cu3-Cu4 paddlewheel dimers in the crystal structure of dehydrated STAM-17-OEt.[5] The closest Cu-O contacts are highlighted. (c, d) ^{13}C (9.4 T, 40 kHz MAS, 298 K) NMR spectra of (c) dehydrated STAM-17-OEt,[5] and (d) dehydrated STAM-1. (e) ^{13}C (9.4 T, 37.5 kHz MAS, 298 K) NMR spectrum of dehydrated HKUST-1.

Table 1. ^{13}C pNMR parameters for STAM-17-Me. Errors start in the last quoted significant figure.

Assignment	δ_{iso} at 298 K (ppm)	T_1 at 298 K / ms	T_2* at 298 K / ms
C2	–60.4	1.1	0.11
C3	221.3	5.3	0.59
C4, C5	179.3	9.5	0.86
C6	24.8	16	1.1

Table 2. ^{13}C pNMR parameters for STAM-17-OMe. Errors start in the last quoted significant figure.

Assignment	δ_{iso} at 298 K (ppm)	T_1 at 298 K / ms	T_2* at 298 K / ms
C2	–57.4	1.5	0.12
C3	216.4	9.1[a]	0.66
C4	165.7	8.8	0.60
C5	218.7	9.1[a]	1.1
C6	50.0	18	1.0

[a] These resonances are overlapped under the experimental conditions used for T_1 measurement and only a combined value was determined for both species.

Table 3. ^{13}C pNMR parameters for STAM-1. Errors start in the last quoted significant figure.

Assignment	δ_{iso} at 298 K (ppm)	T_1 at 298 K / ms	T_2* at 298 K / ms
C2	–53.8	1.3	0.15
C3	226.7	5.1	0.64
C4	181.7	8.5	0.74
C5	174.1	15	1.6
C6	177.7	14	0.93
C7	48.5	26	1.0